RSC Sustainability

ROYAL SOCIETY OF CHEMISTRY

PAPER

View Article Online
View Journal | View Issue

Cite this: *RSC Sustainability*, 2024, **2**, 1837

Utilization of CO_2-captured poly(allylamine) as a polymer surfactant for nanoarchitecture production in a closed CO_2 cycle†

Eri Yoshida

Intensified global warming, due to increased atmospheric CO_2, is an urgent worldwide issue. To reduce atmospheric CO_2 concentrations, various absorbents have been developed for its effective capture and storage. However, the CO_2 stores could become another form of waste unless they are utilized as valuable materials. This study focuses on the utilization of a CO_2-captured absorbent as a surfactant to produce nanoarchitectures in a closed loop of the CO_2 cycle. Poly(allylamine) (PAA) effectively captured carbonic acid (CA) in an aqueous medium upon the introduction of gaseous CO_2, loading the ammonium bicarbonate onto the side chains. The molecular weight of PAA showed no significant difference in its ability and efficiency to capture CA. The CA-captured PAA released the CA at room temperature upon introducing N_2 due to the transformation of the bicarbonate into carbamate – a process that was reversible and repeatable with alternating introductions of CO_2 and N_2. The CA-captured PAA was converted into a polymer surfactant through the partial ion exchange of the bicarbonate with sodium dodecyl sulfate (SDS). At concentrations below the SDS critical micelle concentration (CMC), the surfactant self-assembled into monodisperse nanospheres, which transformed into worm-like morphologies upon increasing the polymer concentration. The utilization of the CO_2 store, in this study employing ion exchange, involves releasing bicarbonate, which is recyclable as a CO_2 source. This CO_2 capture-storage-utilization in a closed loop shows promise in diminishing CO_2 emissions.

Received 10th March 2024
Accepted 3rd May 2024

DOI: 10.1039/d4su00121d

rsc.li/rscsus

Sustainability spotlight

To address accelerated global warming, effective CO_2 storage and its utilization are crucial for reducing CO_2 emissions. Although much attention has been paid to improving the CO_2 capacity and regenerability of absorbents, this study focuses not only on the effective capture of CO_2 as carbonic acid but also on the utilization of the CO_2-captured absorbent for a surfactant that produces nanoarchitectures. The breakthrough in CO_2 storage lies in utilizing the CO_2 stores in its closed loop employing simple ion exchange, which facilitates industrial innovations in CO_2 utilization and promises to diminish CO_2 emissions. This study particularly emphasizes its alignment with SDG 13 (Climate Action), SDG 14 (Life Below Water), and SDG 9 (Industry, Innovation, and Infrastructure).

Introduction

Accelerated CO_2 concentrations have been exacerbating global warming.[1,2] The rise in global temperatures, due to increased CO_2 emissions, has generated heatwaves, leading to destructive droughts and extensive wildfires.[3] These frequent wildfires have further increased CO_2 emissions, creating a vicious cycle of warming. A rise in ocean temperatures has caused sea levels to rise by melting ice sheets,[4–7] resulting in the reduction of terrestrial habitats[8,9] and changes in marine ecosystems.[10–13] These environmental changes have led to significant losses in biodiversity[13,14] and impacts on the global economy.[15,16] If CO_2 emissions continue to increase at the current rate, it is anticipated that the global temperatures will rise at an even more accelerated pace by 2035,[2] which will lead to further environmental, ecological and economic damage.

To reduce atmospheric CO_2, numerous efforts employing various innovative methods have been made, including the reduction of CO_2 through photochemical,[17–19] electrochemical[20–23] and biological approaches[24] into valuable compounds such as formic acid, formaldehyde, methanol and hydrocarbons; the co-reduction with nitrate to produce urea;[25] the incorporation of CO_2 into polymer main chains *via* copolymerization;[26–28] and composting with biomass.[29,30] These methods offer new avenues for fixing CO_2 and producing materials composed of it. However, these methods have not yet been effective enough to significantly reduce atmospheric CO_2 concentrations.

Department of Applied Chemistry and Life Science, Toyohashi University of Technology, 1-1 Hibarigaoka, Tempaku-cho, Toyohashi 441-8580, Japan. E-mail: yoshida.eri.gu@tut.jp

† Electronic supplementary information (ESI) available. See DOI: https://doi.org/10.1039/d4su00121d

Currently, carbon capture and storage (CCS) technology, including direct air capture,[31] is the most promising approach to address global warming.[32,33] CCS involves three distinct processes: capturing CO_2, compressing it for transportation and injecting it deep underground for its permanent storage in a dense phase under high pressure.[34] Efficient CO_2 absorption and subsequent desorption to regenerate the absorbents are crucial for executing all these processes in an energy-efficient manner. Numerous systems for CO_2 absorption and desorption have been developed to improve CO_2 capacity, absorbent regenerability, cyclic stability and durability. These systems involve the use of physical[35–37] or chemical solvent dissolving absorbents,[38] solid absorbents,[39–41] gas separation membranes,[42–45] calcium looping[46,47] and inherent CO_2 trapping.[48] The chemical solvent-based systems are convenient, widely available, easily prepared and well-studied for CCS. Various amines for the chemical solvents have been designed and fabricated to enhance the performance of CO_2 absorption and desorption.[38,49–52] The performance often depends on the amine class and its CO_2 absorption mechanism; tertiary amines simply undergo an acid–base reaction with CO_2 to produce their ammonium bicarbonate or carbonate due to the lack of hydrogen atoms in the amino group.[53,54] On the other hand, primary and secondary amines covalently bond with CO_2 to form the ammonium carbamate, which often requires a much higher temperature to release the CO_2.[55–57]

PAA is an effective CO_2 absorbent and offers many advantages over low-molecular-weight amines, including non-volatility, high CO_2 capacity,[58] thermal stability,[33] resistance to oxidative degradation,[59] durability against high-pressure gas streams[38] and low regeneration energy.[60] Regarding thermal stability and resistance to oxidative degradation,[61–64] PAA, which is loaded with primary amines on its side chains, is more suitable for CO_2 sorption than poly(ethylenimine) (PEI) that incorporates secondary amines in its main chain, although PAA is less effective in CO_2 adsorption capacity and amine efficiency than PEI.[65] Additionally, the commercial availability and easy modifiability of PAA allow for broad design and conversion into unique materials,[66] including not only CO_2 absorbents[67,68] but also polymer surfactants[69] and biocompatible polymers for medical use.[70] Material design aimed at replacing existing functional materials with PAA that has stored CO_2, facilitates industrial utilization of CO_2-captured absorbents. Utilizing CO_2 stores is environmentally significant because allowing them to increase without utilization could cause additional pollution from the CO_2 stores, further contributing to global environmental degradation.

With the aim of effectively utilizing CO_2-captured absorbents, this study demonstrated the efficient capture of CO_2 as carbonic acid (CA) using PAA, followed by the sequential use of the CO_2-captured PAA as a polymer surfactant to produce nanoarchitectures. This paper describes the reversible capture and release of CA by PAA and the conversion of the CA-captured PAA into a polymer surfactant that self-assembles into nanoarchitectures through ion exchange.

Experimental

Instrumentation

Electroconductivity (EC) and pH were measured using a Hanna Instruments HI99300N portable EC/TDS/°C meter and a HI991002N portable pH/ORP/°C meter, respectively. ^{1}H and ^{13}C NMR measurements were conducted using Jeol ECS500 and ECS400 FT NMR spectrometers. The viscosity was measured at 25 °C using an A&D SV-10 vibro viscometer equipped with an Eyela digital Uni Ace UA-100 temperature circulator. UV spectra were obtained at 25 °C using a Shimadzu UV-160A UV-Vis recording spectrophotometer, equipped with an Eyela NCB-1200 temperature circulator. FT-IR spectra were obtained using a Jasco FT/IR-4100 Fourier transform infrared spectrometer. Light scattering measurements were performed at 25 °C with a Photal Otsuka Electronics ELS-8000 electrophoretic light scattering spectrophotometer, equipped with a system controller, an ELS controller and a He–Ne laser operating at $\lambda = 632.8$ nm.

Materials

PAAs with weight-average molecular weights (M_w) of 1600, 5000 and 15 000 were supplied by Nittobo Co., Ltd as their aqueous solutions; 15 wt% solutions for PAAs with $M_w = 1600$ and 15 000, and a 20 wt% solution for that with $M_w = 5000$. Poly(allylamine hydrochloride) (PAH-Cl), with $M_w = 1600$, 5000 and 15 000, was also supplied by Nittobo Co., Ltd as aqueous solutions; a 34 wt% solution for $M_w = 1600$, 40 wt% solution for $M_w = 5000$ and 50 wt% solution for $M_w = 15\,000$. 1,6-Diaminohexane (DA-Hex), purchased from Tokyo Chemical Industry, was purified by distillation over calcium hydride under reduced pressure. Ammonium bicarbonate, ammonium carbonate and ammonium carbamate were purchased from Sigma-Aldrich and used as received. Sodium dodecyl sulfate (SDS), purchased from Kishida Chemical, and sodium ethyl sulfate (SES), obtained from Tokyo Chemical Industry, were used as received. Ultrapure water was obtained using a Merck Milli-Q® Integral MT-5 water purification system. CO_2 with over 99.995% vol purity and N_2 with over 99.9995% vol purity were purchased from Taiyo Nippon Sanso Corporation.

CO_2 capture by PAA; general procedure

Ultrapure water (20 mL) was poured into PAA with $M_w = 15\,000$ (10.161 g as a 15 wt% solution containing 1.524 g (26.7 mmol) of the allylamine unit, AA, and 8.637 g of water), resulting in an initial AA concentration of $[AA]_0 = 0.932$ mol L^{-1}. CO_2 was introduced by bubbling at a flow rate of 300 mL min^{-1}, using a flow meter, into the solution contained in a 50 mL round-bottom flask situated in a water bath maintained at 25 °C, with stirring. The pH of the solution was measured at designated times. At these times, a portion of the solution (1 mL) was extracted using a syringe and diluted with water (14 mL) to facilitate an EC measurement, owing to the upper limitation of the EC meter.

Isolation of CA-captured PAA

The solution of CA-captured PAA with $M_w = 15\,000$, obtained by the procedure mentioned above using 3.010 g of PAA (as

a 15 wt% solution containing 7.91 mmol of AA) and 5.9 mL of water with CO_2 introduced for 30 min, was freeze-dried for 1 h at room temperature, followed by 3.5 h at 25 °C in a water bath, resulting in a white powder (0.910 g) with a 97% yield based on the bicarbonate. Following the same procedure, PAA with M_w = 5000 (2.253 g as a 20 wt% solution containing 7.89 mmol of AA) and 6.6 mL of water produced a powder (0.818 g) with an 87% yield. Similarly, PAA with M_w = 1600 (3.004 g as a 15 wt% solution containing 7.89 mmol of AA) and 5.9 mL of water resulted in a powder (0.888 g) with a 94% yield.

Release of CA from the CA-captured PAA by N_2 introduction

A solution ($[AA]_0$ = 0.932 mol L^{-1}) of CA-captured PAA was prepared using 5.078 g of PAA with M_w = 15 000 (as a 15 wt% solution containing 13.3 mmol of AA) and 10 mL of water, by introducing CO_2 for 1 h. N_2 was then introduced into the solution with stirring at a flow rate of 300 mL min^{-1} for 1 h, after which the solution was subjected to NMR measurements.

Ion exchange of the CA-captured PAA with SDS

A solution of CA-captured PAA was prepared using PAA with M_w = 15 000 (283.0 mg as a 15 wt% solution containing 0.744 mmol of AA) and 207 mL of water, with CO_2 introduced for 30 min. The solution was then divided into 20 mL sample bottles in 10 mL portions while under the CO_2 flow. SDS (103.7 mg, 0.360 mmol) was dissolved in 10 mL of water to prepare a solution with a concentration of 3.60 × 10^{-2} mol L^{-1}. Next, the SDS solution (0.1 mL, 3.60 × 10^{-3} mmol) was added to the CA-captured PAA solution (10 mL, 3.59 × 10^{-2} mmol) with stirring on a water bath at 25 °C. The resulting mixture, with a molar ratio of SDS/AA = 0.1, was subjected to UV and light scattering measurements at 25 °C. Following the same procedure, mixtures with other ratios were prepared using the designated amounts of the SDS solution. Light scattering measurements were performed at an angle θ = 90°. The hydrodynamic diameter (D_h) of the polymer was determined using cumulant analysis, while the number conversion distribution of the D_h was obtained using Marquadt analysis.[71]

FE-SEM observations

The CA-captured PAA solution ($[AA]_0$ = 3.59 × 10^{-3} mol L^{-1}) and SDS solution (3.60 × 10^{-2} mol L^{-1}) were used. The SDS solution (0.26 mL, 9.38 × 10^{-3} mmol) was added to the CA-captured PAA solution (5.2 mL containing 1.87 × 10^{-2} mmol of AA) at 25 °C on a water bath, with stirring. The mixture ([AA] = 3.42 × 10^{-3} mol L^{-1}) was maintained at 25 °C with stirring for 5 min, and then left to stand at 25 °C for an additional 5 min. A drop of the mixture, thus prepared, was placed onto a cover glass (18 × 18 mm) and then put in an oven set at 25 °C for drying. The aggregates on the cover glass were subjected to FE-SEM measurements at 0.7 kV without coating. Morphologies and sizes of the aggregates were determined by the FE-SEM observations, while the size distribution was calculated as previously reported.[72]

Results and discussion

CO_2 capture and release by PAA

To control the reversible capture and release of CO_2 by PAA, the ability to capture CA in an aqueous medium was evaluated using pH and EC variability. As gaseous CO_2 was introduced by bubbling into an aqueous solution of PAA (M_w = 15 000), the solution immediately turned opaque within a few seconds, then gradually became clear and completely homogeneous in 5 min. During the very early stage, a slight amount of the ammonium carbamate and carbonate,[73,74] which are in equilibrium,[75] electrostatically cross-links the polymer chains, causing gelation; however, the gel is disrupted by further capture of CA (Fig. 1). This reasoning agrees with the mechanism of reactions between CO_2 and aqueous ammonia, which is based on substance stability as inferred from their reaction enthalpies.[76,77] Ammonia (NH_3) initially reacts with gaseous CO_2 to produce ammonium carbamate, NH_2COONH_4 (eqn (1)). This compound then converts into ammonium carbonate, $(NH_4)_2CO_3$, in the presence of water (eqn (2)).

As CO_2 reacts with water to generate carbonic acid (CA), NH_3 captures the CA to produce ammonium carbonate (eqn (3)) and ammonium bicarbonate, NH_4HCO_3 (eqn (4)). The bicarbonate further converts into ammonium carbamate by reacting with remaining ammonia (eqn (5)). With the introduction of additional CO_2, increasing the concentration of CA, the ammonium carbonate and carbamate eventually convert into ammonium bicarbonate (eqn (6) and (7)). All these reactions are in equilibrium; however, the forward reactions are preferred because the products are more stable than the starting substances, achieving reduced energy levels by releasing heat. The transition from ammonium carbamate to bicarbonate *via* carbonate agrees with the phase diagram of the CO_2–NH_3–H_2O system.[78]

$$2NH_3 + CO_2 \rightleftarrows NH_2COONH_4,\ \Delta H_{rx} = -72.32\ \text{kJ mol}^{-1} \quad (1)$$

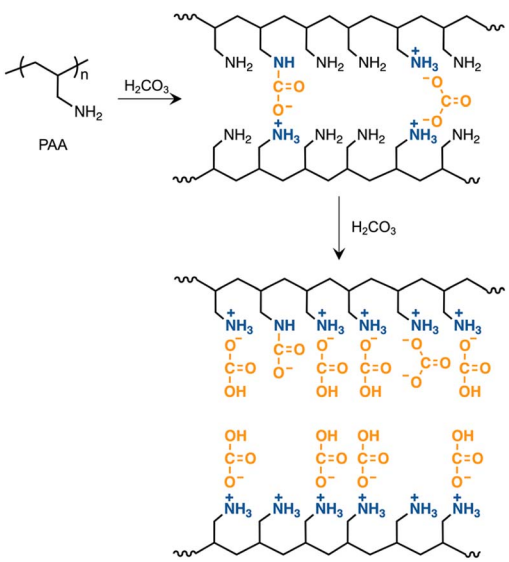

Fig. 1 Gelation of PAA by the carbamate/carbonate generation.

$$NH_2COONH_4 + H_2O \rightleftarrows (NH_4)_2CO_3, \quad \Delta H_{rx} = -28.90 \text{ kJ mol}^{-1} \quad (2)$$

$$2NH_3 + CO_2 + H_2O \rightleftarrows (NH_4)_2CO_3, \ \Delta H_{rx} = -101.22 \text{ kJ mol}^{-1} \quad (3)$$

$$NH_3 + CO_2 + H_2O \rightleftarrows NH_4HCO_3, \ \Delta H_{rx} = -64.26 \text{ kJ mol}^{-1} \quad (4)$$

$$NH_4HCO_3 + NH_3 \rightleftarrows NH_2COONH_4, \ \Delta H_{rx} = -8.06 \text{ kJ mol}^{-1} \quad (5)$$

$$(NH_4)_2CO_3 + CO_2 + H_2O \rightleftarrows 2NH_4HCO_3, \quad \Delta H_{rx} = -26.88 \text{ kJ mol}^{-1} \quad (6)$$

$$NH_2COONH_4 + CO_2 + 2H_2O \rightleftarrows 2NH_4HCO_3, \quad \Delta H_{rx} = -56.20 \text{ kJ mol}^{-1} \quad (7)$$

Fig. 2 and 3 show ^{1}H and ^{13}C NMR spectra, respectively, for the CA-captured PAA. The proton signal at 2.60 ppm (Fig. 2a) for the methylene attached to the amino group shifted to 2.96 ppm (Fig. 2b) due to the protonation of the amino group by CA. In ^{13}C NMR, the bicarbonate (HCO_3^-) was confirmed at 160.4 ppm (Fig. 3b and S1†),[54,79] coexisting with a small amount of the carbamate (NH_2COO^-) detected at 164.5 ppm. Isolating the CA-captured PAA by freeze-drying reduced the intensity of the bicarbonate signal, suggesting a partial release of the CA under reduced pressure during freeze-drying (Fig. 3c), transforming the bicarbonate into carbonate. However, the PAA remains in the ammonium form based on no change in ^{1}H NMR (Fig. 2c), implying that the PAA retained the CA even in its solid state. FT-IR verified the presence of bicarbonate, carbonate and carbamate in the isolated PAA. As can be seen in Fig. 4, the PAA showed four characteristic absorptions at 1640, 1567, 1486 and 1439 cm^{-1}, which are attributed to C–O/C=O stretching. Ammonium carbamate exhibited these absorptions at 1630, 1543, 1459 and 1406 cm^{-1}. These absorptions overlapped with those of bicarbonate/carbonate C–O/C=O stretching, since ammonium bicarbonate and ammonium carbonate had absorptions at 1604 and 1605 cm^{-1}, respectively. However, the PAA exhibited absorption at 2575 cm^{-1}, originating from the N–H stretching of the ammonium cation ($-NH_3^+$) with a bicarbonate or carbonate counter anion, while ammonium bicarbonate showed it at 2590 cm^{-1} and ammonium carbonate also at 2590 cm^{-1}.

The capture of CA charges PAA, producing its polyelectrolyte. Fig. 5 shows variations in EC and pH upon introducing CO_2 into solutions of PAAs with different molecular weights (M_w = 1600, 5000 and 15 000). The introduction of CO_2 initially caused a decrease in EC due to the temporary gelation; thereafter, the EC increased with the duration of CO_2 exposure and reached

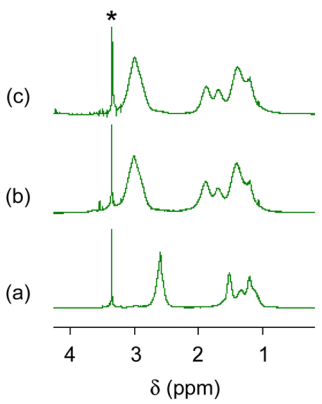

Fig. 2 ^{1}H NMR spectra. (a) PAA with M_w = 15 000, (b) the CA-captured PAA in solution after CO_2 introduction for 1 h and (c) the CA-captured PAA isolated. Solvent: D_2O. *CH_3OH standard.

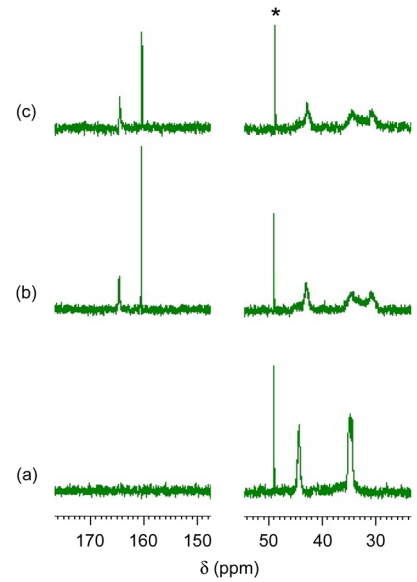

Fig. 3 ^{13}C NMR spectra. (a) PAA with M_w = 15 000, (b) the CA-captured PAA in solution after CO_2 introduction for 1 h and (c) the CA-captured PAA isolated. Solvent: D_2O. *CH_3OH standard.

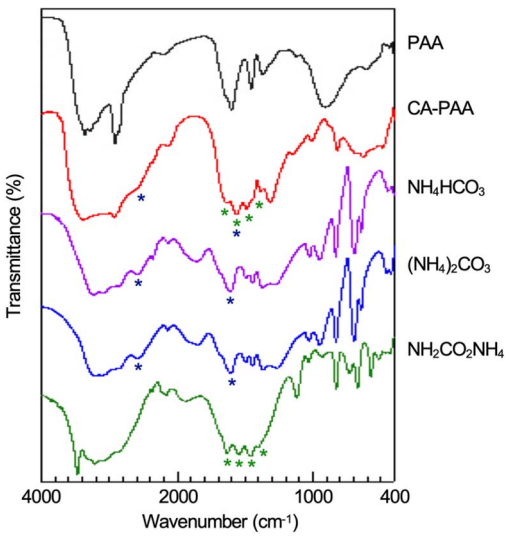

Fig. 4 FT-IR spectra of PAA (M_w = 15 000), isolated CA-captured PAA (CA-PAA), ammonium bicarbonate, ammonium carbonate and ammonium carbamate.

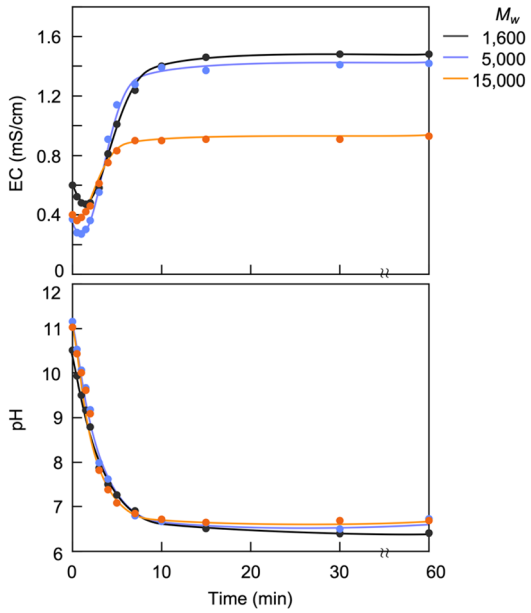

Fig. 5 Variations in EC and pH of PAA solutions on introducing CO_2. $[AA]_0 = 0.932$ mol L^{-1} for the pH measurement and 0.0621 mol L^{-1} for the EC.

steady states. During the CO_2 introduction, the PAAs showed no difference in pH variability, suggesting no difference in their ability and efficiency to capture CA. However, the steady-state EC value linearly decreased with the logarithm of the molecular weight ($\log M_w$) (Fig. 6a). The decrease in EC with the increased molecular weight was attributed to the increased viscosity of the electrolyte solution. The restriction of molecular movement by binding the amino groups to the high-molecular-weight polymer chain reduced the EC. This inverse correlation of EC with the molecular weight is characteristic of polyelectrolytes, as evidenced by PAH-Cl, which also exhibited a linear decrease in EC *versus* $\log M_w$ (Fig. 6b). For the same molecular weight, the CA-captured PAA had a lower EC than PAH-Cl due to its lower ion conductivity: 44.5×10^{-4} m^2 S mol^{-1} for HCO_3^-, 69.3×10^{-4} m^2 S mol^{-1} for $1/2CO_3^{2-}$ and 76.31×10^{-4} m^2 S mol^{-1} for Cl^-.[80]

PAA is effective for capturing CA, compared to low-molecular-weight amino compounds. Fig. 7 shows variations in the pH of solutions using three different amines: TM-Hex, DA-Hex and PAA ($M_w = 1600$). The primary amines captured CA more efficiently than the tertiary amine due to their less steric hindrance and greater hydrophilicity. Furthermore, the polymeric amine grasped CA more effectually than DA-Hex because it produced a much lower pH, although it reduced EC due to the restriction of molecular movement. Binding the amines involves more amine molecules in interacting with a CA molecule, resulting in effective capture of CA (Fig. 8).

The CA-captured PAA exhibited differences in discharging CA between its solid and liquid states. DSC analysis revealed that the polymer began to release CO_2 at 68.6 °C and completed this upon continued heating (Fig. 9). Whereas the CA-captured

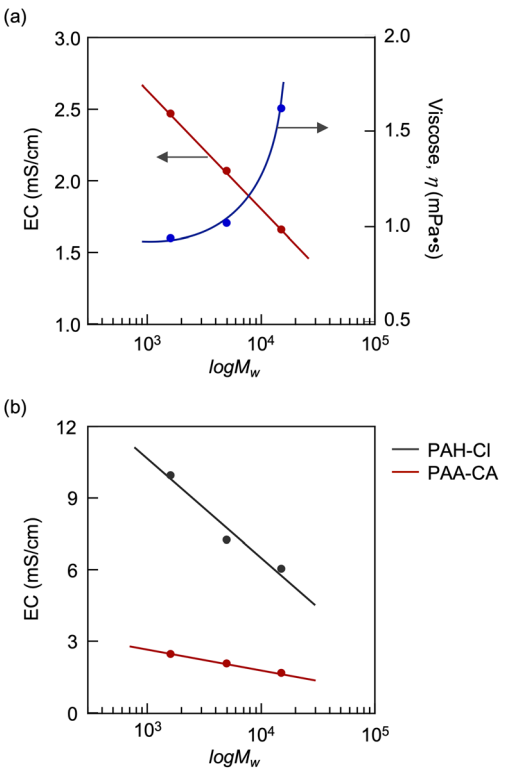

Fig. 6 (a) Plots of the steady-state EC value and viscosity *versus* the molecular weight of PAA. (b) Plots of EC *versus* the molecular weight for the CA-captured PAA (PAA-CA) and PAH-Cl. [AA] = [AH-Cl] = 0.116 mol L^{-1}.

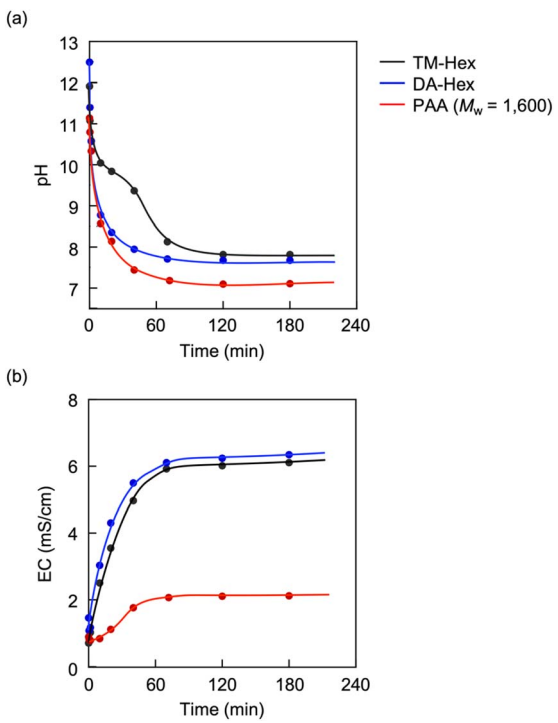

Fig. 7 Variations in (a) pH and (b) EC upon introducing CO_2 into solutions of TM-Hex,[54] DA-Hex and PAA. $[NR_2]_0 = 2.63$ mol L^{-1} for the pH measurement and 0.117 mol L^{-1} for the EC. R = CH_3 for TM-Hex and H for DA-Hex and PAA. CO_2 flow rate = 250 mL min^{-1}.

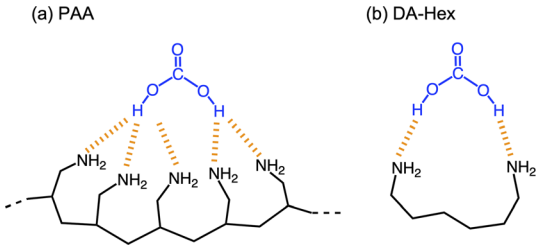

Fig. 8 Mechanism for the more efficient capture of CA by PAA compared to DA-Hex.

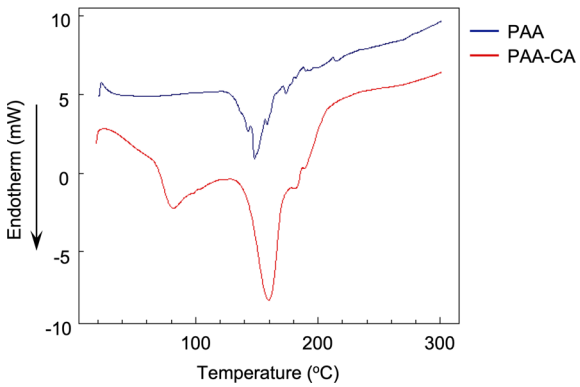

Fig. 9 DSC spectra of the CA-captured PAA (PAA-CA) and PAA. M_w = 15 000.

PAA in a solid state required heating to discharge the CA, the polymer in solution released it at room temperature upon introducing N_2. After N_2 introduction for 1 h, the solution showed only the signal at 164.5 ppm in ^{13}C NMR (Fig. 10b),

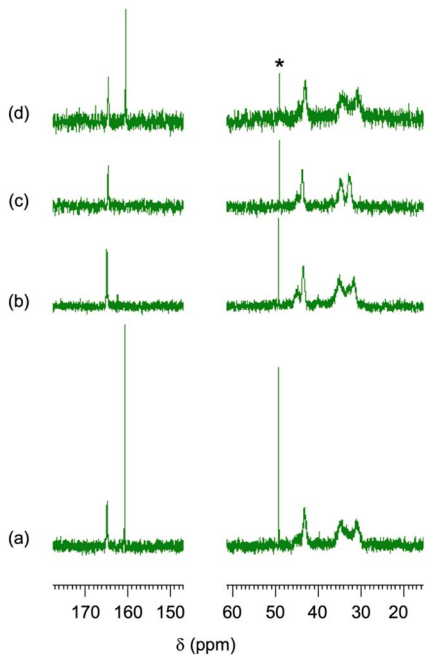

Fig. 10 ^{13}C NMR spectra of the CA-captured PAA: (a) after introduction of CO_2 for 1 h, (b) N_2 for 1 h at 25 °C, (c) N_2 for 1 h at 60 °C and (d) second CO_2 for 1 h. M_w = 15 000. Solvent: D_2O. *CH_3OH standard.

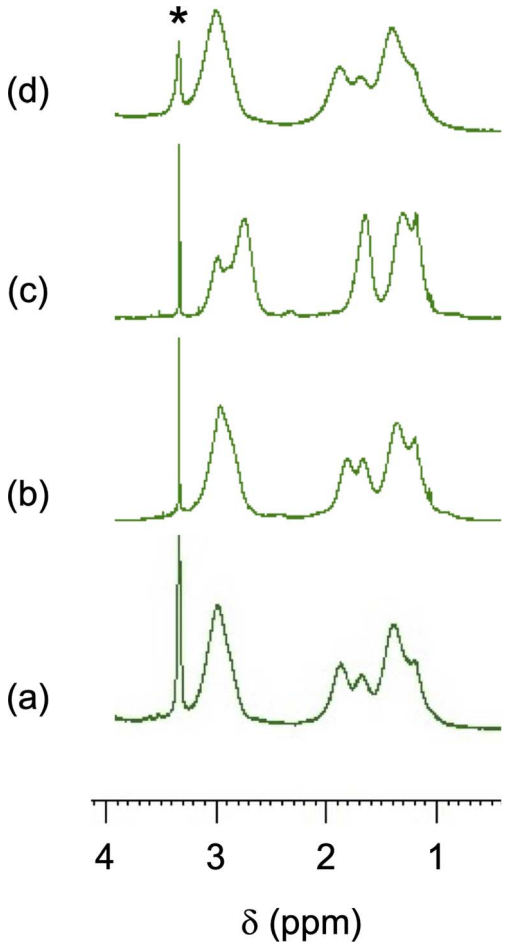

Fig. 11 ^1H NMR spectra of the CA-captured PAA: (a) after introduction of CO_2 for 1 h, (b) N_2 for 1 h at 25 °C, (c) N_2 for 1 h at 60 °C and (d) second CO_2 for 1 h. M_w = 15 000. Solvent: D_2O. *CH_3OH standard.

indicating that the bicarbonate converted into carbamate, thereby releasing CO_2. This release produced no change in the chemical shift of the methylene protons in ^1H NMR (Fig. 11b), suggesting the absence of CA-free allylamine units. Raising the temperature reduced the intensity of the carbamate carbon signal (Fig. 10c), while the methylene proton signal partially shifted to that of the original PAA (Fig. 11c), indicating that the CA-captured PAA partially discharged the CO_2 from the carbamate to produce CA-free allylamine units. The polymer captured CA again upon a second CO_2 introduction, producing

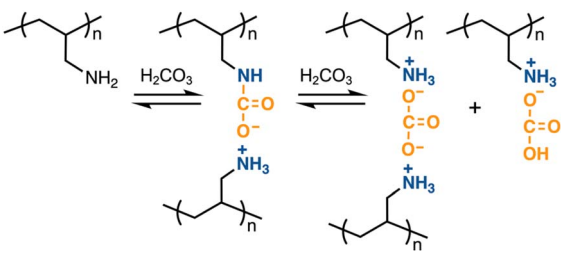

Fig. 12 Reversible transitions between PAA and the ammonium carbamate, and between the carbamate and bicarbonate/carbonate.

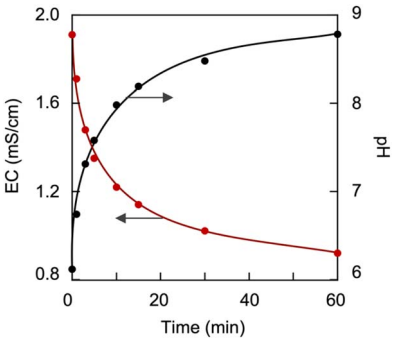

Fig. 13 Variations in EC and pH of the CA-captured PAA solution on introducing N_2. $[AA]_0 = 0.116$ mol L^{-1}, $M_w = 15\,000$.

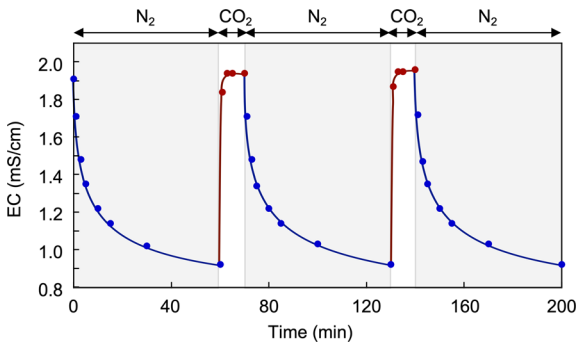

Fig. 14 Repetitive changes in EC and pH of the CA-captured PAA by alternating CO_2/N_2 introductions. $[AA]_0 = 0.116$ mol L^{-1}, $M_w = 15\,000$.

bicarbonate and carbonate (Fig. 10d and 11d). Thus, the transitions between PAA and the ammonium carbamate, and between the carbamate and bicarbonate/carbonate, are reversible (Fig. 12).

However, the carbamate-to-bicarbonate/carbonate transition is a much lower-energy process that proceeds at room temperature. Fig. 13 shows variations in EC and pH of the CA-captured PAA solution upon introducing N_2, based on the conversion of the bicarbonate to carbamate. After introducing N_2 for 1 h, the EC and pH reached their steady states. The decrease in EC was linked to the increase in pH, indicating that the CA was removed as gaseous CO_2 from the solution.

This transition was completely reversible and repeatable by alternating CO_2/N_2 introductions, as evidenced by the excellent hysteresis in the EC changes upon repeated introductions (Fig. 14).

Conversion of CA-captured PAA into polymer surfactant

Ammonium bicarbonate readily undergoes ion exchange due to its weak electrostatic interaction between the ammonium cation and bicarbonate anion. It has been reported that a polymer loading the ammonium bicarbonate derived from hindered secondary amine, ion-exchanged with poly(sodium 4-styrenesulfonate) to produce polymer complexes with ribbon-like or sheet-like morphologies.[81] The present study investigated partial ion exchange with SDS to convert the CA-captured PAA

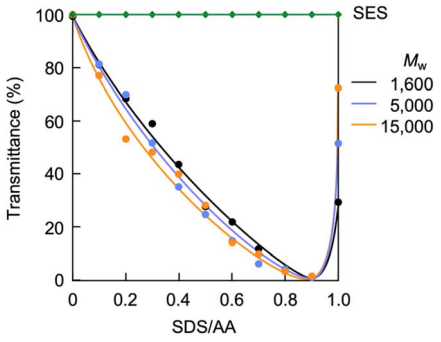

Fig. 15 Variation in transmittance of the polymer solution *versus* the SDS/AA ratio. $[AA]_0 = 3.59 \times 10^{-3}$ mol L^{-1}. SES for PAA ($M_w = 15\,000$).

into a polymer surfactant. By this conversion, the PAA randomly loads the dodecyl groups on its side chains, producing a random copolymer-like surfactant. Amphiphilic random copolymers, readily available by one-step polymerization, self-assemble into micellar nanospheres.[82,83] SDS is an anionic low-molecular-weight surfactant and serves as a cation exchanger and a modifier of micelle surfaces.[84,85] SDS has a low critical micelle concentration (CMC) of 8.3×10^{-3} mol L^{-1} at 25 °C.[86–88] Below this CMC, this study explored the ion exchange of the CA-captured PAA with SDS at 25 °C. UV analysis revealed that the CA-captured PAA aggregated in the presence of SDS. The variations in transmittance of the polymer solutions are shown in Fig. 15, with the concentration of $[AA]_0 = 3.59 \times 10^{-3}$ mol L^{-1} *versus* the SDS/AA ratio. As a result of increasing the SDS/AA ratio, the transmittance at a 400 nm wavelength decreased. The ion exchange between the bicarbonate anion and dodecyl sulfate loaded the hydrophobic dodecyl groups onto the CA-captured PAA chain, causing its aggregation. At an SDS/AA ratio of 1.0, the transmittance suddenly increased due to the precipitation of the aggregates. The polymer released all the bicarbonate anions through the ion exchange with an equivalent amount of dodecyl sulfate, forming insoluble aggregates. It is evident that the dodecyl groups on the polymer induced aggregation, since SES produced no change in transmittance for the polymer solution. The ethyl chain is too short to induce polymer aggregation.

Light scattering studies demonstrated that the polymer loading with the dodecyl groups self-assembled into

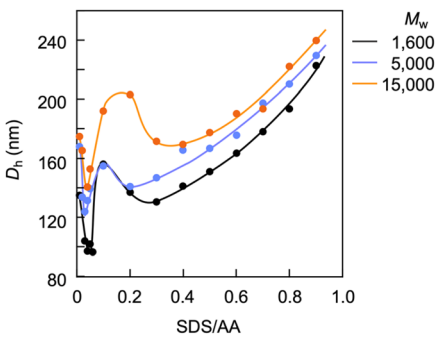

Fig. 16 Variation in hydrodynamic diameter of the CA-captured PAA *versus* the SDS/AA ratio. $[AA]_0 = 3.59 \times 10^{-3}$ mol L^{-1}.

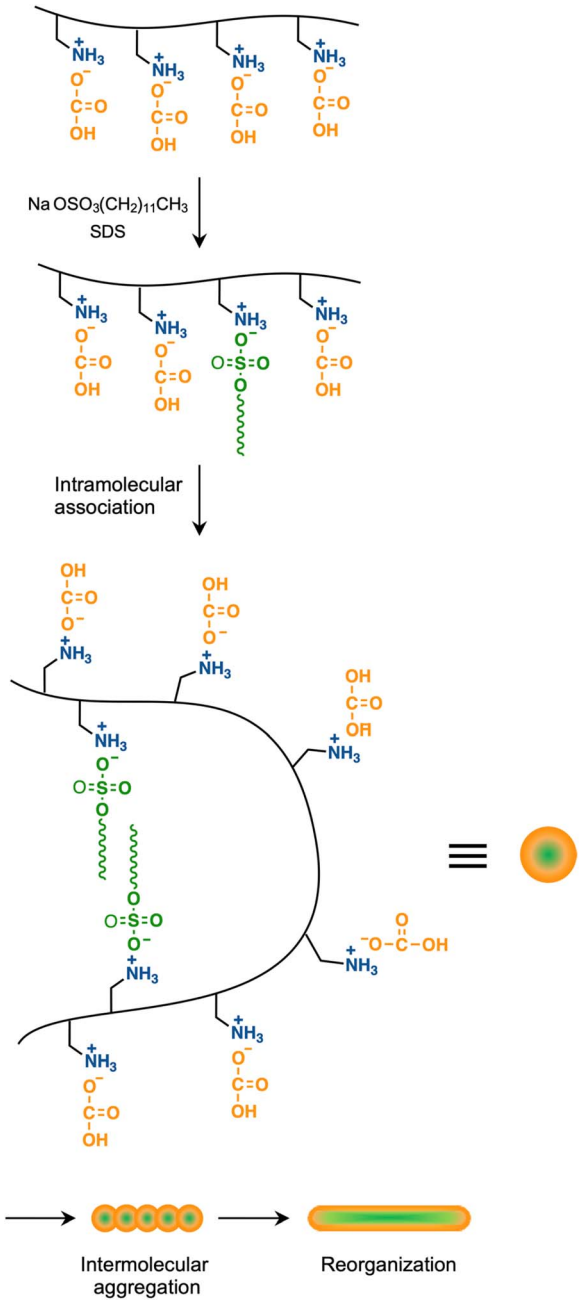

Fig. 17 Association states of the polymer for different amount of SDS.

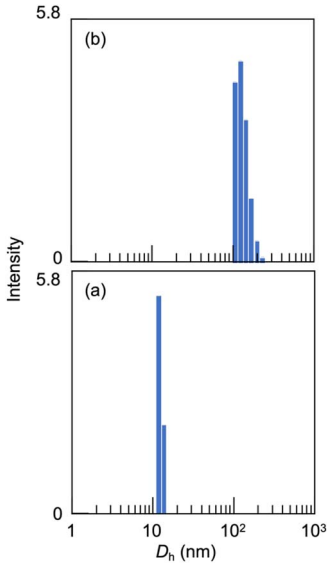

Fig. 18 The number conversion distributions in light scattering: (a) the isolated polymer at SDS/AA = 0.01 and (b) aggregates at SDS/AA = 0.1. M_w = 15 000, $[AA]_0 = 3.59 \times 10^{-3}$ mol L^{-1}.

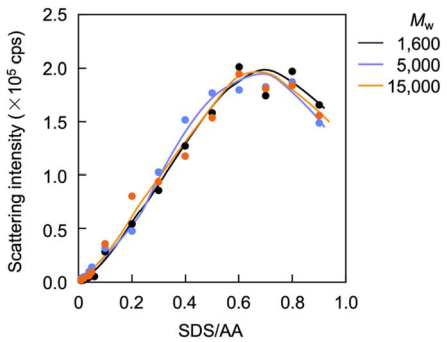

Fig. 19 Variation in scattering intensity of the polymer solution *versus* the SDS/AA ratio. $[AA]_0 = 3.59 \times 10^{-3}$ mol L^{-1}.

nanoparticles. Fig. 16 shows the variation in hydrodynamic diameter (D_h) of the CA-captured PAA upon adding SDS. The D_h immediately decreased with the addition of a small amount of SDS, then rapidly increased with more SDS. The hydrodynamic size decreased again with further SDS addition and finally increased due to continued addition of SDS. This up-and-down change in the D_h with increasing SDS reflects different association states of the polymer. A small number of dodecyl groups induce intramolecular association of the polymer, shrinking the polymer chain and causing a reduction in the hydrodynamic size (Fig. 17). The polymer chains aggregated with each other due to the increased number of dodecyl groups, resulting in an increase in the hydrodynamic size. A further increase in the number of dodecyl groups disrupts the intramolecular association, altering it to intermolecular aggregation, which causes the second decrease in D_h. This switch from the intramolecular association to the intermolecular aggregation involves reorganization of the self-assembly, leading to a gradual increase in the D_h with further addition of SDS. SDS shows no self-assembly in the absence of the CA-captured polymer, being below its CMC. The dodecyl groups significantly induced the self-assembly of the polymer by locating on the polymer side chains. Even with the SDS concentration at 3.60×10^{-4} mol L^{-1}, which is 23 times lower than the CMC and corresponds to a 0.1 ratio to AA, all the polymer chains participated in the self-assembly, and there were no isolated polymer chains based on the number conversion distribution analysis in the light scattering (Fig. 18). The isolated polymer was 12.7 nm in diameter, aggregating to a size of 192.2 nm at the 0.1 ratio. Up to an SDS/AA ratio of 0.6, the scattering intensity of the polymer

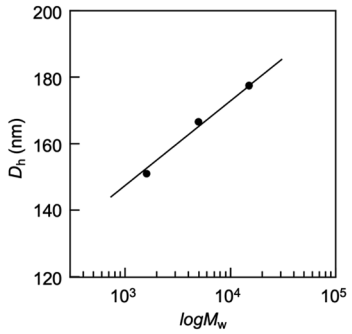

Fig. 20 Plots of the hydrodynamic diameter of the aggregates *versus* the molecular weight of PAA. SDS/AA = 0.5, $[AA]_0 = 3.59 \times 10^{-3}$ mol L^{-1}.

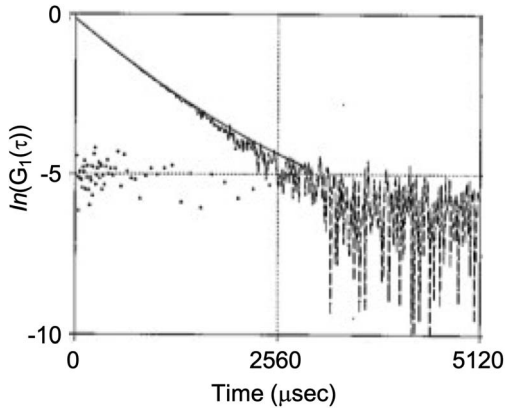

Fig. 21 Variation in $G_1(\tau)$ with time for the polymer solution. $M_w = 15\,000$. SDS/AA = 0.5. $[AA]_0 = 3.59 \times 10^{-3}$ mol L^{-1}.

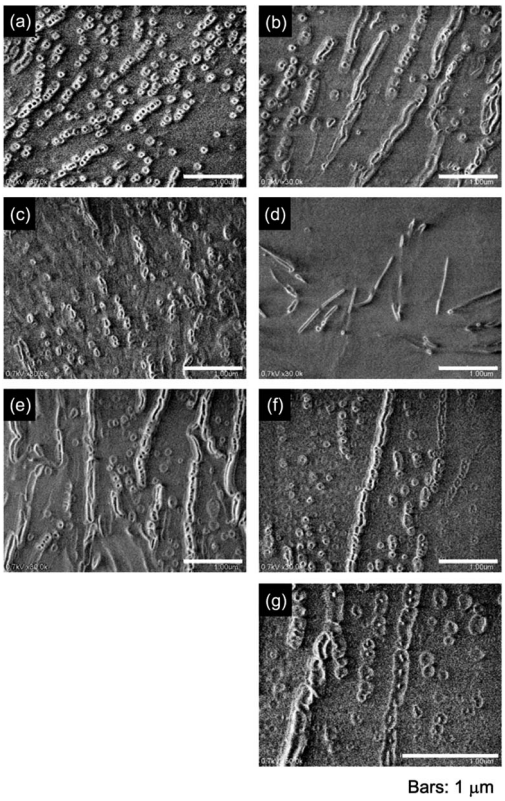

Fig. 22 FE-SEM images of the aggregate morphologies for the polymer surfactants with the molecular weight: (a and b) $M_w = 15\,000$, (c and d) 5000 and (e–g) 1600. (a, c and e) $[AA]_0 = 3.42 \times 10^{-3}$ mol L^{-1} and (b, d, f and g) 1.03×10^{-2} mol L^{-1}.

solution increased (Fig. 19); however, it decreased beyond this ratio due to the highly dodecyl-loaded polymers precipitating. The aggregates are stabilized below the medium SDS/AA ratio by the ammonium bicarbonate surrounding the hydrophobic dodecyl core. Fig. 20 displays a linear correlation between the D_h of the aggregates at SDS/AA = 0.5 and the log M_w of the polymer. The size of the aggregates lay in a range of 150 to 180 nm, depending on the molecular weight of the polymer. The normalized time correlation function of the scattering field, $G_1(\tau)$, revealed that the CA-captured PAA produced monodisperse spherical aggregates. For monodisperse spherical particles, $G_1(\tau)$ displays a single exponential decay with time.[89] As shown in Fig. 21, the polymer with $M_w = 15\,000$ and SDS/AA = 0.5 exhibited a linear decay of $\ln(G_1(\tau))$ with time, indicating the formation of monodisperse spherical aggregates due to the intramolecular self-assembly of the long polymer chain. As the molecular weight decreased, the $\ln(G_1(\tau))$ decay deviated from a linear line (Fig. S2†). The low-molecular-weight polymer had the potential to form non-spherical or polydisperse nanoparticles due to their random intermolecular aggregation.

FE-SEM observations demonstrated that the high-molecular-weight polymer aggregated into spherical monodisperse nanoparticles (Fig. 22a). The particles had a number-average diameter (D_n) of 106.7 nm, which is much smaller than the D_h observed in light scattering due to the observation of the aggregates shrunk by drying. The size distribution (D_w/D_n) was obtained by calculation using the weight-average diameter (D_w), calculated as $D_w = \Sigma D_i^4/\Sigma D_i^3$, according to a previous study.[72] The D_w was calculated to be 112.9 nm for the spherical particles, leading to a size distribution of $D_w/D_n = 1.06$, indicative of monodisperse particles when it is considered that a size distribution of $D_w/D_n = 1.00$ is perfect for monodisperse particles. The particles transformed into a worm-like morphology with an increase in the polymer concentration (Fig. 22b). At a high concentration, the intramolecular aggregates connected with each other in line, causing the transformation into worm-like particles. Lower molecular weight polymers more readily self-assembled into worm-like particles even at low concentrations due to their intermolecular aggregation (Fig. 22c–f). Furthermore, the M_w 1600 polymer produced vesicle-like nanoparticles at a high concentration (Fig. 22g). The shorter chain polymer is more hydrophilic, increasing the hydrophilicity of the internal core, resulting in self-assembly into vesicles. Not only the vesicles but also the spherical and worm-like particles are nano-sized capsules with micellar structures, since they were produced by the self-assembling of the polymer surfactants. These nanoarchitectures are stabilized with the bicarbonate on the surface of their outer shells, which have the potential to serve as nanocarriers for drugs and genes in

delivery systems, releasing them in response to bicarbonate concentrations in the blood. The polymer surfactant developed in this study also has the potential to perform highly in the polymer alternating gas (PAG) process used in enhanced oil recovery (EOR). In this process, the polymer facilitates oil movement toward production wells by alternating with CO_2 to displace oil.[90–92] The conversion of the CA-captured PAA into the polymer surfactant is accompanied by CO_2 release, which can be controlled by adjusting the ratio of the ion exchanger. The ion exchange in water causes the surfactant to self-assemble into nanoobjects, which are expected to effectively displace oil when used in the PAG injection method. The simultaneous generation of nanoobjects and CO_2 release in water could improve the water alternating gas injection method[93] and simplify the PAG method, leading to more effective EOR.

Conclusions

This study demonstrated the effective capture of CO_2 as carbonic acid using PAA and utilization of the CO_2-captured PAA for a polymer surfactant to produce nanoarchitectures. PAA captures carbonic acid more effectively than low-molecular-weight amines due to its polymeric amine structure, where more amino groups assist in capturing carbonic acid. The capture of carbonic acid produces electrolytes, the electroconductivity of which is inversely proportional to the molecular weight of the polymer, due to increased viscosity. PAA reversibly and repeatably releases carbonic acid in an aqueous medium at room temperature through alternating introductions of CO_2 and N_2, relying on the equilibrium between ammonium bicarbonate/carbonate and carbamate. The carbonic acid-captured PAA is converted into a polymer surfactant to produce spherical and worm-like nanoarchitectures by undergoing partial ion exchange between the bicarbonate anion and dodecyl sulfate. The bicarbonate anions released from the PAA by the ion exchange are a source of CO_2, forming a closed loop of CO_2 in the utilization of the CO_2-captured absorbent. The conversion of the CO_2-captured polymer can create versatile surfactants by selecting various ion exchangers. This material design, employing CO_2-captured absorbents within a closed loop, facilitates industrial uses of these absorbents, promising to reduce CO_2 emissions.

Conflicts of interest

There are no conflicts to declare.

Acknowledgements

This work was supported by the Japan Society for the Promotion of Science (JSPS) Grant-in-Aid for Scientific Research (Grant Number 23K04533).

References

1 M. T. McCulloch, A. Winter, C. E. Sherman and J. A. Trotter, *Nat. Clim. Change*, 2024, **14**, 171–177.
2 A. Mani, T. Budd and E. Maine, *RSC Sustainability*, 2024, **2**, 903–927.
3 C. G. Bousfield, D. B. Lindenmayer and D. P. Edwards, *Nat. Geosci.*, 2023, **16**, 1145–1150.
4 D. K. Hutchinson, L. Menviel, K. J. Meissner and A. M. Hogg, *Nat. Commun.*, 2024, **15**, 1026.
5 H. Pang, W. Zhang, S. Wu, T. M. Jenk, M. Schwikowski and S. Hou, *Sci. Bull.*, 2024, **69**, 375–381.
6 K. A. Hapsari, T. Jennerjahn, S. H. Nugroho, E. Yulianto and H. Behling, *Global Change Biol.*, 2022, **28**, 3459–3479.
7 P. Blanchon, A. Eisenhauer, J. Fietzke and V. Liebetrau, *Nature*, 2009, **458**, 881–885.
8 A. Dada, R. Almar and P. Morand, *Sci. Rep.*, 2024, **14**, 890.
9 S. A. Kulp and B. H. Strauss, *Nat. Commun.*, 2019, **10**, 4844.
10 S. Lee, R. Lumpkin, F. Gomez, S. Yeager, H. Lopez, F. Takglis, S. Dong, W. Aguiar, D. Kim and M. Baringer, *Nat. Commun. Earth Environ.*, 2023, **4**, 69.
11 N. R. Bates and R. J. Johnson, *Nat. Commun. Earth Environ.*, 2020, **1**, 33.
12 M. McLean, D. Mouillot, A. A. Maureaud, T. Hattab, M. A. MacNeil, E. Goberville, M. Lindegren, G. Engelhard, M. Pinsky and A. Auber, *Curr. Biol.*, 2021, **31**, 4817–4823.
13 S. E. Moffitt, T. M. Hill, P. D. Roopnarine and J. P. Kennett, *Proc. Natl. Acad. Sci. U.S.A.*, 2015, **112**, 4684–4689.
14 G. Gao, L. Song, Y. Zhang and H. Chu, *Soil Biol. Biochem.*, 2024, **191**, 109348.
15 W. W. L. Cheung, R. Watson and D. Pauly, *Nature*, 2013, **497**, 365–369.
16 C. Arbués, T. Chatzivasileiadis, O. Ivanova, S. Storm, F. Bosello and T. Filatova, *Sci. Rep.*, 2024, **14**, 126.
17 S. Yin, Y. Zhou, Z. Liu, H. Wang, X. Zhao, Z. Zhu, Y. Yan and P. Huo, *Nat. Commun.*, 2024, **15**, 437.
18 M. He, Z. Fang, P. Wang, Y. You and Z. Li, *ACS Sustainable Chem. Eng.*, 2023, **11**, 12194–12217.
19 K. Wang, Z. Hu, P. Yu, A. M. Balu, K. Li, L. Li, L. Zeng, C. Zhang, R. Luque, K. Yan and H. Luo, *Nano-Micro Lett.*, 2024, **16**, 1–17.
20 Z. Xie, E. Huang, S. Garg, S. Hwang, P. Liu and J. G. Chen, *Nat. Catal.*, 2024, **7**, 98–109.
21 T. Kawawaki, T. Okada, D. Hirayama and Y. Negishi, *Green Chem.*, 2024, **26**, 122–163.
22 Y. Hua, C. Zhu, L. Zhang and F. Dong, *Materials*, 2024, **17**, 600.
23 B. Chang, H. Pang, F. Raziq, S. Wang, K. Huang, J. Ye and H. Zhang, *Energy Environ. Sci.*, 2023, **16**, 4714–4758.
24 A. Molino, S. Mehariya, D. Karatza, S. Chianese, A. Iovine, P. Casella, T. Marino and D. Musmarra, *Energies*, 2019, **12**, 2806.
25 Y. Li, S. Zheng, H. Liu, Q. Xiong, H. Yi, H. Yang, Z. Mei, Q. Zhao, Z. Yin, M. Huang, Y. Lin, W. Lai, S. Dou, F. Pan and S. Li, *Nat. Commun.*, 2024, **15**, 176.
26 C. Deacy, A. F. R. Kilpatrick, A. Regoutz and C. K. Williams, *Nat. Chem.*, 2020, **12**, 372–380.
27 S. Klaus, M. W. Lehenmeier, C. E. Anderson and B. Rieger, *Coord. Chem. Rev.*, 2011, **255**, 1460–1479.
28 Y. Qin, X. Sheng, S. Liu, G. Ren, X. Wang and F. Wang, *J. CO_2 Util.*, 2015, **11**, 3–9.

29 E. Woods, V. R. Berrio, Y. Qiu, P. Berlin, N. Clauser and W. J. Sagues, *RSC Sustainability*, 2024, **2**, 621–625.
30 S. Stegenta-Dabrowska, E. Sygula, M. Bednik and J. Rosik, *Materials*, 2024, **17**, 563.
31 S. Chowdhury, Y. Kumar, S. Shrivastava, S. K. Patel and J. S. Sangwai, *Energy Fuels*, 2023, **37**, 10733–10757.
32 X. Yu, C. O. Catanescu, R. E. Bird, S. Satagopan, Z. J. Baum, L. M. L. Diaz and Q. A. Zhou, *ACS Omega*, 2023, **8**, 11643–11664.
33 A. A. Olajire, *Energy*, 2010, **35**, 2610–2628.
34 D. Kearns, H. Liu and C. Consoli, *Technology Readiness and Costs of CCS*, Global CCS Institute, 2021, pp. 1–50.
35 W. L. Theo, J. S. Lim, H. Hashim, A. A. Mustaffa and W. S. Ho, *Appl. Energy*, 2016, **183**, 1633–1663.
36 Y. Mohammed, M. Samah, A. Mohamed and G. Sabina, *Int. J. Eng. Res.*, 2014, **3**, 742–744.
37 N. Hedin, L. Andersson, L. Bergström and J. Yan, *Appl. Energy*, 2013, **104**, 418–433.
38 T. N. Borhani and M. Wang, *Renewable Sustainable Energy Rev.*, 2019, **114**, 109299.
39 T. S. Nguyen, N. A. Dogan, H. Lim and C. T. Yavuz, *Acc. Chem. Res.*, 2023, **56**, 2642–2652.
40 C. Kim, Y. Ha and M. Choi, *Acc. Chem. Res.*, 2023, **56**, 2887–2897.
41 M. A. Alkhabbaz, R. Khunsupat and C. W. Jones, *Fuel*, 2014, **121**, 79–85.
42 J. Wei, Y. Ma, Z. Qin, Z. Jin, Y. Jin, L. Yang, L. Yao, W. Jiang, Y. Deng, Y. Huang, H. Zhao, J. Dong, L. Deng and Z. Dai, *Sep. Purif. Technol.*, 2023, **320**, 124182.
43 Y. Pu, Z. Yang, V. Wee, Z. Wu, Z. Jiang and D. Zhao, *J. Membr. Sci.*, 2020, **641**, 119912.
44 K. Kim, J. Lee and J. Lee, *J. Membr. Sci.*, 2020, **598**, 117796.
45 T. H. H. Shiue, S. M. Chang and G. Leggett, *Int. J. Environ. Sci. Technol.*, 2022, **19**, 4237–4250.
46 J. Chen, L. Duan, Y. Ma, Y. Jiang, A. Huang, H. Zhu, H. Jiao, M. Li, Y. Hu, H. Zhou, Y. Xu, F. Donat, M. A. Naeem and O. Krocher, *Fuel*, 2023, **334**, 126630.
47 F. M. Baena-Moreno, D. Mei, H. Leion and D. Pallares, *Biomass Bioenergy*, 2023, **176**, 106918.
48 W. Chan, T. Morosuk, X. Li and H. Li, *Energy Convers. Manage.*, 2023, **294**, 117607.
49 A. Gautam and M. K. Mondal, *Fuel*, 2023, **334**, 126616.
50 M. Bernhardsen and H. K. Knuutila, *Int. J. Greenhouse Gas Control*, 2017, **61**, 27–48.
51 R. Guo, G. Li, Y. Liu and W. Pan, *Energy Fuels*, 2023, **37**, 15429–15452.
52 R. Zhang, Y. Li, X. He, Y. Niu, C. Li, M. W. Amer and F. Barzagli, *Sep. Purif. Technol.*, 2023, **316**, 123810.
53 G. F. Versteeg and W. P. M. Van Swaaij, *Chem. Eng. Sci.*, 1988, **43**, 587–591.
54 E. Yoshida, *SCIREA J. Chem.*, 2020, **5**(2), 12–29.
55 B. Aghel, S. Sahraie and E. Heidaryan, *Energy*, 2020, **201**, 117618.
56 G. F. Versteeg and W. P. M. Van Swaaij, *Chem. Eng. Sci.*, 1988, **43**, 573–585.
57 G. F. Versteeg, L. A. J. Van Dijck and W. P. M. Van Swaaij, *Chem. Eng. Commun.*, 1996, **144**, 113–158.
58 J. Kothandaraman, A. Goeppert, M. Czaun, G. A. Olah and G. K. S. Prakash, *Green Chem.*, 2016, **18**, 5831–5838.
59 J. Zhang, Y. Qiao, W. Wang, R. Misch, K. Hussain and D. W. Agar, *Energy Procedia*, 2013, **37**, 1254–1261.
60 Y. Shen, C. Jiang, S. Zhang, J. Chen, L. Wang and J. Chen, *Appl. Energy*, 2018, **230**, 726–733.
61 M. Varghese and G. N. Karanikolos, *Int. J. Greenhouse Gas Control*, 2020, **96**, 103005.
62 D. Wang, X. Wang and C. Song, *ChemPhysChem*, 2017, **18**, 3163–3173.
63 S. Bali, T. T. Chen, W. Chaikittisilp and C. W. Jones, *Energy Fuels*, 2013, **27**, 1547–1554.
64 W. Chaikittisilp, R. Khunsupat, T. T. Chen and C. W. Jones, *Ind. Eng. Chem. Res.*, 2011, **50**, 14203–14210.
65 W. Chaikittisilp, R. Khunsupat, T. T. Chen and C. W. Jones, *Ind. Eng. Chem. Res.*, 2011, **50**, 14203–14210.
66 A. Koutsianos, L. B. Hamdy, C. Yoo, J. J. Lee, M. Taddei, J. M. Urban-Klaehn, J. Dryzek, C. W. Jones, A. R. Barron and E. Andreoli, *J. Mater. Chem. A*, 2021, **9**, 10827–10837.
67 D. Saravanakumar, J. Song, N. Jung, H. Jirimali and W. Shin, *ChemSusChem*, 2012, **5**, 634–636.
68 M. A. Alkhabbaz, R. Khunsupat and C. W. Jones, *Fuel*, 2014, **121**, 79–85.
69 E. Yoshida, *Colloid Polym. Sci.*, 2010, **288**, 1321–1325.
70 E. Apuzzo, M. Agazzi, S. E. Herrera, A. Picco, G. Rizzo, C. Chavero, D. Bianchi, P. Smaldini, M. L. Cortez, W. A. Marmisolle, G. Padula, A. Seoane, M. L. Alomar, M. P. Denofrio, G. Docena and O. Azzaroni, *ACS Appl. Bio Mater.*, 2023, **6**, 4714–4727.
71 D. W. Marquadt, *J. Soc. Ind. Appl. Math.*, 1963, **11**, 431–441.
72 S. Kobayashi, H. Uyama, I. Yamamoto and Y. Matsumoto, *Polym. J.*, 1990, **22**, 759–761.
73 C. K. Ahn, H. W. Lee, Y. S. Chang, K. Han, J. Y. Kim, C. H. Rhee, H. D. Chun, M. W. Lee and J. M. Park, *Int. J. Greenhouse Gas Control*, 2011, **5**, 1606–1613.
74 E. Carretti, L. Dei, P. Baglioni and R. G. Weiss, *J. Am. Chem. Soc.*, 2003, **125**, 5121–5129.
75 N. Wen and M. H. Brooker, *J. Phys. Chem.*, 1995, **99**, 359–368.
76 F. Qin, S. Wang, I. Kim, H. F. Svendsen and C. Chen, *Int. J. Greenhouse Gas Control*, 2011, **5**, 405–412.
77 J. T. YehT, K. P. Resnik, K. Rygle and H. W. Pennline, *Fuel Process. Technol.*, 2005, **86**, 1533–1546.
78 V. Darde, K. Thomsen, W. J. M. van Well and E. H. Stenby, *Energy Procedia*, 2009, **1**, 1035–1042.
79 F. Mani, M. Peruzzini and P. Stoppioni, *Green Chem.*, 2006, **8**, 995–1000.
80 D. R. Lide, *CRC Handbook of Chemistry and Physics*, CRC Press, Boca Raton, 76th edn, 1995, pp. 5-90–5-92.
81 E. Yoshida, *Carbon Capture Sci. Technol.*, 2022, **2**, 100038.
82 I. Sadeghi, J. Kronenberg and A. Asatekin, *ACS Nano*, 2018, **12**, 95–108.
83 S. Imai, Y. Hirai, C. Nagao, M. Sawamoto and T. Terashima, *Macromolecules*, 2018, **51**, 398–409.
84 R. Klein, M. Kellermeier, D. Touraud, E. Müller and W. Kunz, *J. Colloid Interface Sci.*, 2013, **392**, 274–280.
85 J. B. S. Bonilha, R. M. Z. Georgetto, E. Abuin, E. Lissi and F. Quina, *J. Colloid Interface Sci.*, 1990, **135**, 238–245.

86 G. Tyagi, D. Seddon, S. Khodaparast, W. N. Sharratt, E. S. J. Robles and J. T. Cabral, *Colloids Surf., A*, 2021, **618**, 126414.
87 J. P. Marcolongo and M. Mirenda, *J. Chem. Educ.*, 2011, **88**, 629–633.
88 P. H. Elworthy and K. J. Mysels, *J. Colloid Interface Sci.*, 1966, **21**, 331–347.
89 W. Brown, *Light Scattering Principles and Development*. Clarendon Press, Oxford, 1996, pp. 439–442.
90 S. Prakash, D. Joshi, K. Ojha and A. Mandal, *Energy Fuels*, 2024, **38**(7), 5676–5689.
91 N. Kumar, M. A. Sampaio, K. Ojha, H. Hoteit and A. Mandal, *Fuel*, 2022, **330**, 125633.
92 Y. Yang, W. Li, T. Zhou and Z. Dong, *IOP Conf. Series: Earth Environ. Sci.*, 2018, **113**, 012182.
93 S. Kumar and A. Mandal, *J. Pet. Sci. Eng.*, 2017, **157**, 696–715.